(Received 24 February 2025, Accepted 3 June 2025, Scheduled 17 June 2025)

# A New Design of Tunable Dual Band-Notched UWB Flower-Shaped Antenna Verified by CMA

Azadeh Shahpari[1,*] and Mohsen Shafeghati[2]

[1] *K.N. Toosi University of Technology, Tehran, Iran*
[2] *Satellite Research Institute, Iranian Space Research Center (ISRC), Tehran, Iran*

**ABSTRACT:** In this paper, a tunable ultra-wideband antenna based on slot structures is presented and verified using Characteristic Mode Analysis. The antenna is backed with a partial ground plane and covers the 2.8–13.2 GHz frequency band. In this wide frequency range, satisfactory VSWR and gain are achieved. To avoid interference with wireless local area network WLAN (5.2 to 5.8 GHz) and X-Band satellite links (7.9 to 8.4 GHz), two notches are created using U-shaped and elliptical slots. An important feature of this paper is the use of varactor diode in the elliptical slot to achieve tunable frequencies for the second notched band. By applying different bias voltages, the center frequency of the second notched band is continuously tuned. The antenna performance is verified using modal parameters including modal significance and characteristic angle within the working region of the proposed antenna using the theory of characteristic modes analysis. This antenna is implemented on top of a cost-effective FR4 substrate with a 1 mm thickness. The proposed flower-shaped antenna is compact in size and provides ultra-wide bandwidth. The dimension of the optimized design is $25 \times 35 \times 1\,\text{mm}^3$.

## 1. INTRODUCTION

In recent years, wireless communications have played a crucial role in human life. In wireless applications, ultra-wideband (UWB) systems are extremely important. The US Federal Communications Commission (FCC) proposed 3.1 to 10.6 GHz as the UWB frequency band. This report states that UWB systems must operate in this frequency band with their $-10$ dB bandwidth [1]. An important element in the design of a wireless communication system is antenna. Among the most common applications for UWB antennas are data communication, identification, localization, and sensing. Furthermore, UWB systems can support high data rate communication. A UWB antenna saves space and money by eliminating the need for several narrow-band antennas. Planar monopole antennas are an ideal choice among the numerous types of antennas used in UWB applications due to their simple construction, wide bandwidth, and omnidirectional pattern. A UWB antenna operates in a wide frequency range that may interfere with some narrowband services. An important challenge for UWB antennas is reducing electromagnetic interference with narrow-band communication links, such as WLANs or X-band satellite links (5.15–5.85 GHz) and (7.9–8.4 GHz). The use of a notched-band UWB antenna is a better alternative to integrating band-stop filters with UWB antennas. A variety of methods can cause a notched function, including etching different slot structures from radiating elements [2], using various stubs [3, 4], parasitic resonators [5], and split ring resonators (SRRs) on the back side of the substrate close to the radiating element [6, 7]. Additionally, UWB antennas are available with different numbers of notched functions, such as single, dual, triple, and quadruple notches [8–12]. Different UWB antennas are available such as fixed [2] reconfigurable [13–15], and continuously tunable [16, 17] band-notched frequency. Various notched-band UWB antennas are commonly used to eliminate interference in the frequency range. Among the various types of notched band antennas, tunable structures are especially attractive for the use in UWB wireless systems [18]. A significant challenge involves the design of conventional antennas with a wide frequency range and new functionality, such as tunable notched functions. In this paper, in order to tune the notched band frequency range, a varactor diode is inserted in the slot. There are various slot structures that result in antennas with notched-band characteristics. The radiating patch or ground plane may be etched with different shapes, such as U-shaped or annular slots [19, 20]. The proposed antenna is a cost-effective flower-shaped UWB antenna. The antenna covers the UWB frequency range, but rejects the bands (5.15–5.85 GHz) and (7.9–8.4 GHz) to prevent the interference with WLANs and X-band satellite communications. This rejection is achieved by etching both U-shaped and elliptical slots in the radiating patch. The notched frequency of the U-shaped slot can be modified by varying the length of the slot. The second notched band (7.9–8.4 GHz) can be modified by changing the diameter of the elliptical slot and placing other varactors with different capacitance ranges. It is a new development in the field of ultra-wideband antennas to design an antenna with small dimensions and a wide frequency range, as well as to incorporate tuning functionality into a cost-effective design. The simulation and optimization were performed using Computer Simulation Technology (CST) Microwave Studio [21]. In this design, a bandwidth of 2.8 to 13.2 GHz VSWR $< 2$ is obtained.

* Corresponding author: Azadeh Shahpari (a.shahpari@alumni.kntu.ac.ir).

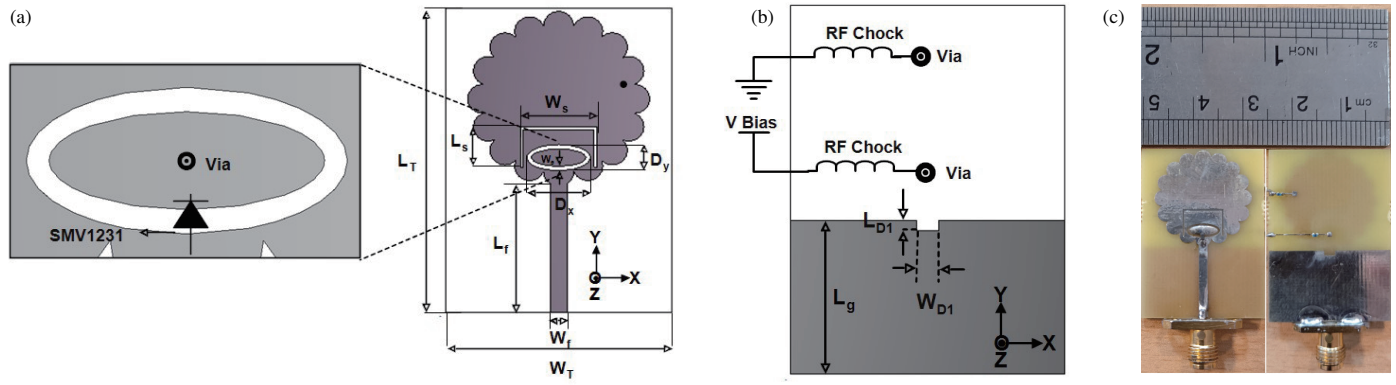


**FIGURE 1**. The proposed antenna structure, (a) top, (b) bottom and (c) the manufactured photograph.

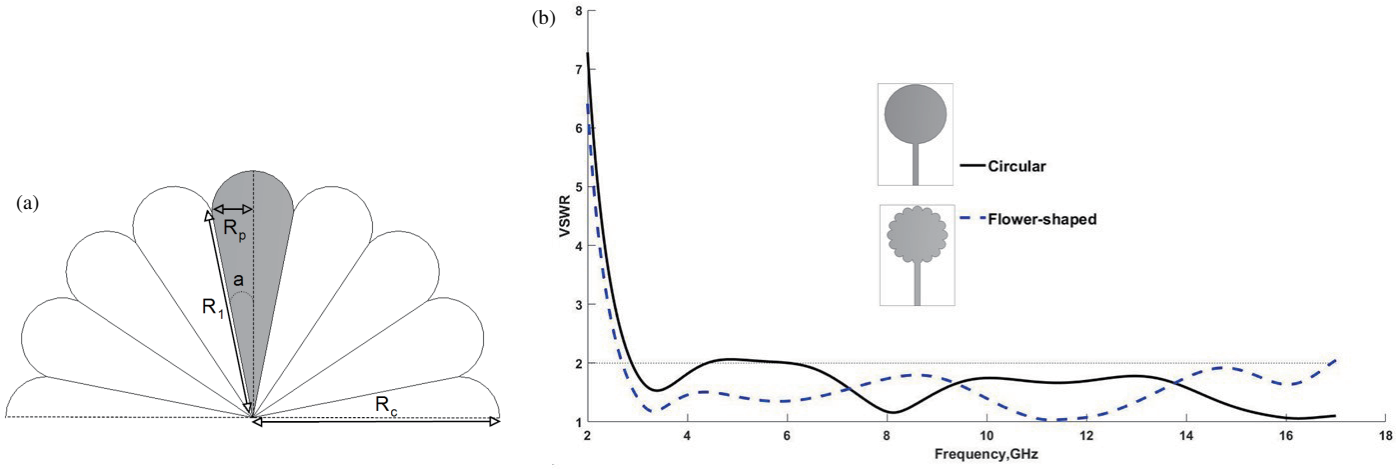


**FIGURE 2**. Schematic view of (a) geometrical parameters for flower-shaped antenna with n-petals and (b) Simulated VSWR for circular patch in comparison with flower shaped patch.

## 2. ANTENNA DESIGN CONSIDERATION

In this paper, a flower-shaped antenna is presented in Fig. 1. This antenna was implemented on a cost-effective FR4 substrate with a relative dielectric constant of $\varepsilon_r = 4.3$ and thickness of 1 mm. The planar printed antenna benefits from more compression and simple structure compared to other types of antennas. As shown in Fig. 1, to obtain the required notched band, U-shaped and elliptical slots are embedded in the radiating patch.

As illustrated in Fig. 1(a) and Fig. 2(a), the proposed antenna structure consists of a circular radiating patch composed of a large circle of radius $R_1$ which is surrounded by sixteen smaller circles of radius $R_p$, forming a flower-shaped patch. The lower band frequency for the circular patch antenna of radius $R_c$ is given as [22]

$$F_L\,(\text{GHz}) = \frac{7.2}{(l + r + g) \times k} \tag{1}$$

where $l = 2R_c$ and $r = \frac{R_c}{4}$ represent the length and effective radius of an equivalent cylindrical monopole antenna, respectively, and $g$ is the gap between ground and circular patch with factor $k = 1.15$ approximately. All the lengths are in cm.

Therefore for $F_L = 2.8\,\text{GHz}$, the suitable radius for circular patch is selected, $R_c = 10.2\,\text{mm}$. As depicted in Fig. 2(a), the angle $a$ is pi/16 and as $R_c = R_1 + R_p$, approximately $R1 = 8.5\,\text{mm}$ and $R_p = 1.7\,\text{mm}$. There are 16 petals in the proposed antenna as depicted in Fig. 2(a). The concentration of the current distribution is on the petal edges more than that on the center of the patch. Therefore, any technique that increases the perimeter will result in a decrease in the lowest resonance frequency. The first resonance frequency $(F_L)$ is inversely proportional to the circumference of the patch [23]

$$\varepsilon_{eff} \approx \frac{\varepsilon_r + 1}{2}$$

then

$$F_L(\text{GHz}) \approx \frac{300}{\text{p}\sqrt{\varepsilon}_{eff}} \tag{2}$$

The perimeter unit in this formula is millimeter, and $\varepsilon_{eff}$ is the effective permittivity. If possible, it would be desirable to increase the circumference of the radiating patch without modifying its outer diameter. A modified version of a conventional circular patch is a flower-shaped patch. This structure can be constructed with different numbers of petals. As shown in Fig. 2(a),

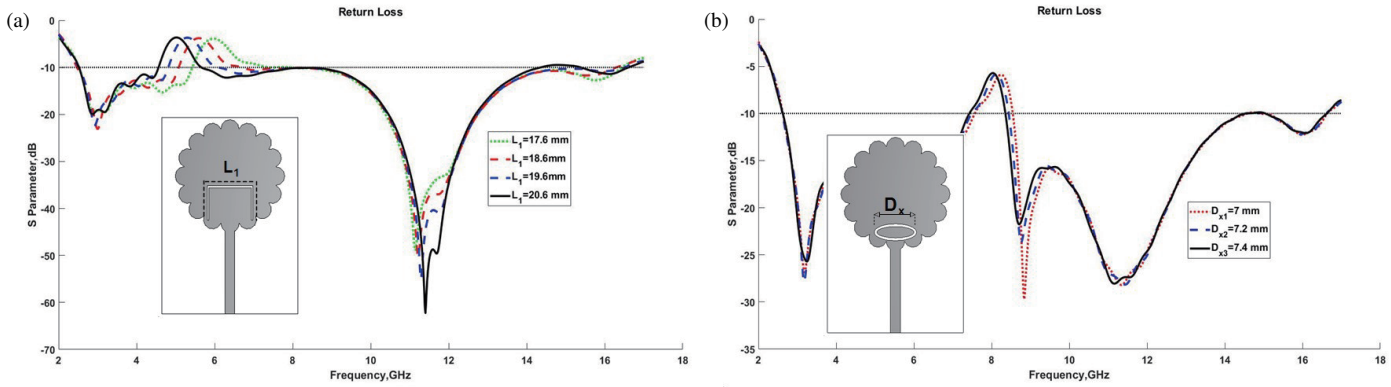


**FIGURE 3**. The simulated $S$-parameter for some values of (a) $L_1$ and (b) $D_x$ in the proposed antenna.

the petal has two radii, $R_p$ edge's radius and $R_1$ main radius. The outer diameter is assumed to be constant ($R_1+R_p$ = cons). If $P_f$ and $P_c$ are the overall perimeters for flower-shaped and circular patches, respectively, the perimeter ratio is calculated by:

$$\frac{P_f}{P_c}=\frac{n}{2}\left(\frac{\tan a}{1+\tan a}\right),\ a=\frac{\pi}{n};\ \text{where } (n=8,16,\ldots) \tag{3}$$

The perimeter of this design with 16 petals increases by about 30% compared to a circular patch with the same outer diameter. With Equation (3), there is a greater than twofold increase in the perimeter of the flower-shaped antenna relative to a circle-shaped antenna of the same radius for a flower with 16 petals as compared to a flower with 8 petals. However, for a larger number of petals, there is no significant increase. Therefore, 16 petals were selected. According to Equation (4), when the perimeter of the antenna is increased, the first resonance frequency is reduced, and the current length path is increased, thereby improving the antenna's impedance bandwidth by producing higher modes [24]. As shown in Fig. 2(b), the first frequency decreases by approximately 20%. As a result of this method, the current distribution at the antenna edge increases, resulting in an increase in gain. A comparison of simulated voltage standing wave ratio (VSWR) values for circular patch and flower-shaped patch antennas at different frequencies is shown in Fig. 2(b).

As shown in Fig. 1, the antenna dimensions have been optimized by CST Microwave Studio. The final antenna design parameters are: $W_T = 25\,\text{mm}$, $L_T = 35\,\text{mm}$, $W_f = 1.8\,\text{mm}$, $L_f = 14.6\,\text{mm}$, $W_{D1} = 2.1\,\text{mm}$, $L_{D1} = 1\,\text{mm}$, $W_s = 8.4\,\text{mm}$, $L_s = 5.1\,\text{mm}$, $D_x = 7.2\,\text{mm}$, $D_y = 3\,\text{mm}$, $R_1 = 8.5\,\text{mm}$, $R_p = 1.7\,\text{mm}$, $L_g = 14.2\,\text{mm}$, $w_e = 0.5\,\text{mm}$.

Therefore, the antenna structure with relevant dimensions is presented. The antenna is implemented on a cost-effective FR4 substrate with the final optimized dimensions $25\times35\times1\,\text{mm}^3$. There is a partial ground plane backing the proposed flower-shaped antenna. Providing a partial ground results in a better frequency response and thus better current distribution. As a result of this improvement in surface current, especially at notch frequencies, a greater amount of energy is concentrated around the slots, preventing radiation at those frequencies. Considering that the length of the ground plane ($L_g$) has a significant effect on the impedance bandwidth, it is optimized for wideband performance. An additional slot was added to the ground plane to improve impedance matching at frequencies. Antenna performance, such as gain at higher frequencies, is enhanced by this slot. The size of the slot was also optimized.

In order to avoid interference with the WLAN frequency band of 5.15–5.825 GHz, the first notch band with a center frequency of 5.4 GHz is chosen. A U-shaped slot was etched from the radiation patch to create this notch. The slot length is calculated by [25].

$$L_1=\frac{c}{2f_{notch}\sqrt{\varepsilon_{eff}}} \tag{4}$$

Here, $L_1 = 2L_s + W_s$ is the length of the slot. The slot length is determined by the center frequency of the notched band. Fig. 3(a) illustrates the results of $S$-parameters simulation for some $L_1$ values. By increasing the slot length from 17.6 to 20.6 mm, the second notched band moves from 5.15 to 5.825 GHz. A preliminary estimate of the U-slot length for the notch with the center at 5.4 GHz is 18.6 mm. In the next step the antenna is simulated and optimized by CST Microwave Studio. In order to obtain the desired antenna bandwidth with the necessary notched bands, parametric values such as antenna dimensions and slot lengths should be optimized.

On the radiating patch, an elliptical slot is etched to obtain the second notched frequency. Therefore, the specified frequency ($f_{notch}$) is rejected in X-band satellite communication links. An elliptical slot with a major diameter of $D_x$, minor diameter of $D_y$ and width $W_e$ is etched out. As shown in Fig. 3(b), the elliptical slot dimensions are calculated through the following equations [26].

$$P=\frac{\lambda_g}{2}=\frac{c}{2f_{notch}\sqrt{\varepsilon_{eff}}}=K_1\pi\left(\frac{D_y}{2}-W_e\right)$$

$$K_1=3\left(1+K_2\right)-\sqrt{\left(3+K_2\right)\left(1+3K_2\right)} \tag{5}$$

$$K_2=\frac{D_x}{D_y}$$

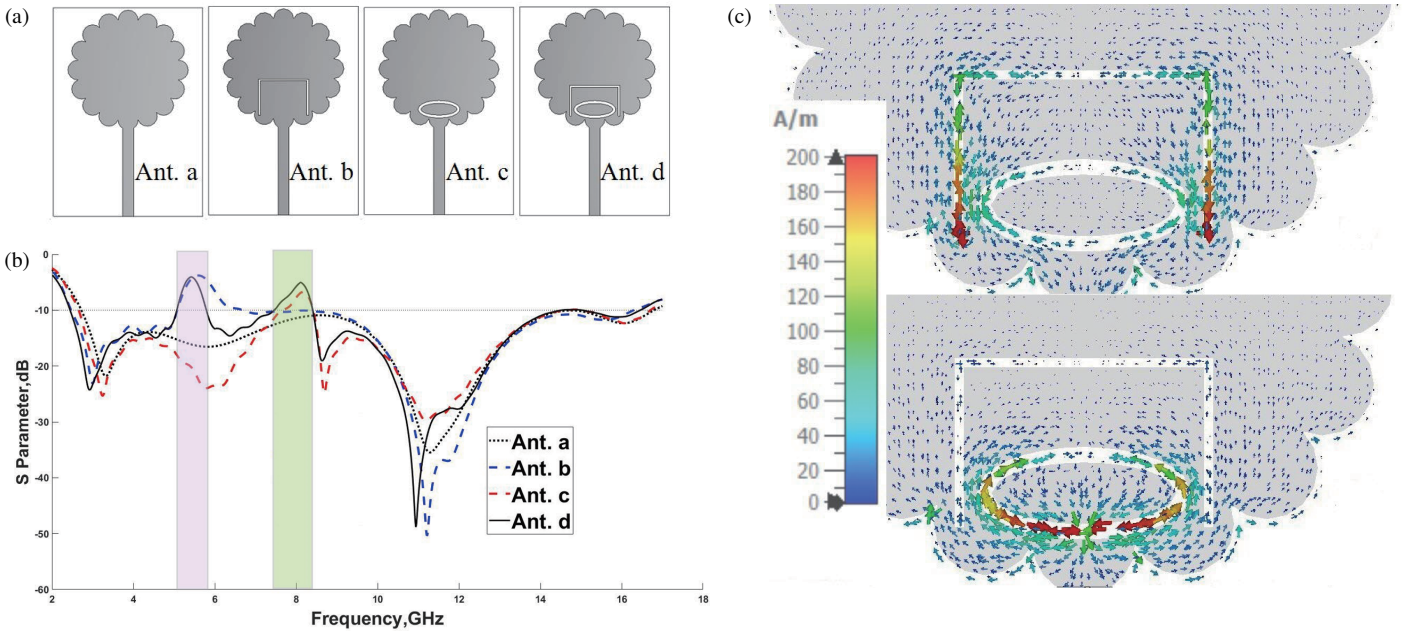


**FIGURE 4**. Four different design steps of the antenna (a) Ant. a: Initial UWB flower antenna. Ant. b: UWB flower-shaped antenna structure with etching out a U-shaped slot from the radiating patch. Ant. c: UWB flowershaped antenna with etching out an elliptical slot from the radiating patch. Ant. d: final double band-notched antenna with U-shaped and elliptical slots. (b) Comparison of four different simulations of the dual band-notched antenna (c) Surface current distribution for the proposed antenna in two notch frequencies (I) 5.4 GHz and (II) 8.15 GHz.

Here, $P$ is the inner circumference of the elliptical slot, $\varepsilon_{eff}$ the effective permittivity, $\lambda_g/2$ the half of the guided wavelength, $K_1$ a parameter related to the ellipticity of the slot, and $K_2$ the ratio of the major to minor diameter of the elliptical slot. The second resonance at 8.15 GHz (falling in the center of (7.9–8.4 GHz)) is achieved by choosing $D_y = 3$ and $W_e = 0.5$. Based on these results, we analytically obtain $K_1 = 3.6$ and $K_2 = 2.4$. Adjusting the frequency of the notch is achieved by changing the length of the slot. Consequently, when the inner circumference of the elliptical slot changes, the frequency of the notch band also changes. As shown in Fig. 3(b), this slot generates various notched frequencies for different lengths of $D_x$. This notched band is centered at 8.15 GHz for $D_x = 7.2$ mm. Due to this, the slot length and therefore the major diameter of the elliptical slot are determined primarily by the preferred center frequency of the notched band. In addition, a varactor diode's capacitance is a fine-tune parameter that contributes to frequency sweeping. The required capacitance determines the range of bias voltages. In CST Microwave Studio, these parameters are used to simulate and optimize the antenna.

Figure 4(a) illustrates the four steps in the antenna design and the corresponding variations in the $S$-parameters of these designs with respect to frequency. As shown in Fig. 4(a), Ant. a illustrates the initial flower-shaped antenna. In order to create the first notched band, a U-shaped slot is etched out as shown on the Ant. b in Fig. 4(a). As a next step, the elliptical slot must be etched out to provide the second notched band (Ant. c). Lastly, both notched bands are obtained as shown on Ant. d. These four step designs are simulated. The variation of $S$-parameters for these steps is depicted in Fig. 4(b).

In addition, the surface current distribution is presented in Fig. 4(c). Additionally, current distributions of two band notched are also simulated in order to analyze how the band notched mechanism actually works. Observations indicate that current distributions are significant in U-shaped and elliptical slots at notched frequencies. Due to the concentration of energy around slot structures, radiation does not occur at those frequencies. As a result, the band-notched characteristics are achieved. In the lower notch frequency (5.4 GHz), the current concentration is at the edges of the U-shaped slot. At this frequency, almost no current is available at the edges of the elliptical slot. A significant surface current is present around the elliptical slot in the second notched band. As a conclusion, looking at Fig. 4, the responsible notched element in the frequency bandwidth is determined.

A varactor diode, SMV1231 [27], is inserted in the elliptical slot to provide tunability around this frequency. The varactor diode is reverse biased using a DC power supply, as it is important to tune the bias voltages using continuous voltage values. An radio frequency (RF) choke is used in this structure to block higher frequencies while passing DC. Consequently, the radiation patch and bias circuit interaction is constrained. The part number of the RF choke is LQ15AN2N9B00 from Murata Co. [28]. The chokes have some limitations such as self-resonance frequency (SRF) that might affect the upper-frequency bandwidth in $S$-parameter measurements. The integration of varactor diode with the bias circuit is shown in Fig. 5(a). In order to minimize the effect of substrate losses due to SMD components, the width and length of the microstrip lines in biasing circuits is optimized using CST Microwave Studio. As illustrated in Fig. 3(b), the varactor diode equivalent circuit consists of pack-

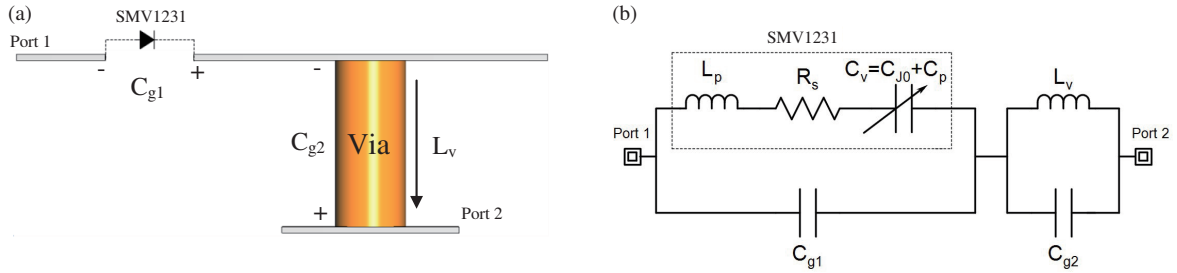


**FIGURE 5**. (a) The integration of the varactor diode with bias circuit. (b) The approximate equivalent circuit of the varactor diode SMV1231 with bias circuit.

age inductance ($L_p = 0.7$ nH), series resistance ($R_s = 2.5\,\Omega$), package capacitance ($C_p = 0.44$ pF), and junction capacitance ($C_{J0}$). Junction capacitance may be tuned from 0.487 pF to 2.35 pF by changing the reverse voltage from 12 V to 0 V [24]. In simulation results with this voltage change, the second notch frequency moves from 7.3 GHz to 8.7 GHz. Fig. 5 illustrates the bias circuit with the varactor diode and its equivalent circuit. As shown in Fig. 5(b) and Equation (4), the slot length and the capacitance range of the varactor diode are the significant factors that determine the center frequency of the second notch. Also as depicted in Fig. 5(a), the other parameters that may affect the second notch are the width of elliptical slot ($W_e$) and substrate thickness which influences $C_{g1}$, $C_{g2}$, and $L_v$.

## 3. NOTCH BEHAVIOR OF PROPOSED UWB ANTENNA VERIFIED BY CHARACTERISTIC MODE ANALYSIS (CMA)

Finding the fundamental modes that contribute to the antenna's radiation and formation of notched bands is significant. Characteristic Mode Analysis (CMA) helps to understand the resonance behavior of the antenna. As a result of an incoming electromagnetic field, the total current flowing through a radiating structure is described as the weighted sum of transverse eigencurrents ($J_n$).

$$J = \sum_{n=m}^{M} \beta_n J_n \tag{6}$$

In this equation, $\beta_n$ represents the modal weight coefficients that calculate the impact of each eigencurrent on the overall current. The total radiated electric field is generated by the total current because each eigencurrent generates its own electric field. An important metric of the CMA is modal significance (MS), which determines each mode's maximum normalized current strength.

$$MS = \left|\frac{1}{1 + j\lambda_n}\right| \tag{7}$$

In this case, $\lambda_n$ is the eigenvalue of the $i$th mode and is related to the eigencurrents using a modal matrix ($[Z]$), as follows:

$$\begin{aligned} [Z] &= [R] + j[X] \\ [X]J_n &= \lambda_n [R] J_n \end{aligned} \tag{8}$$

In this equation, $R$ and $X$ represent the real and imaginary parts of impedance $Z$, respectively. The characteristic angle ($\alpha_n$) is used to describe the phase difference between the electric field and surface current.

$$\alpha_n = 180 - \tan^{-1}(\lambda_n) \tag{9}$$

Based on characteristic mode analysis theory, the dual band notched characteristics of the proposed radiator are examined with regard to the modal significance and characteristic angle [29, 30]. By solving the generalized eigenvalue problem, characteristic modes are obtained. It is considered a good radiator when the modal significance value is greater than 0.7 [26]. In Fig. 7, the modal curves at various frequencies with 10 modes are displayed as the Modal Significance (MS) and Characteristic Angle (CA) responses of the radiator. A second parameter that describes the antenna's radiating performance is Characteristics Angle (CA) that is illustrated in Fig. 7(b). Also, angle values near 180° indicate a good radiating performance for the antenna. The frequencies in which their MS values are more than 0.7 and the CA near 180° are modal bandwidth [30]. According to Fig. 7(a), Modes 12 and 45 have MS values above 0.7 and CA near 180, which identifies them as resonant modes. To address the influence of the of the modes on the radiation pattern, surface current distribution of two modes of the antenna at frequencies of 5.3 GHz and 8.15 GHz is presented in Fig. 6(c). Each mode has a unique surface current distribution. Modification of the antenna structure and feed placement to selectively excite the desired modes illustrates how CMA guides design optimization. Therefore, through Characteristic Mode Analysis, the antenna's performance is verified. As a consequence of the CMA, occurrences of the notches in an antenna's frequency response can sometimes be attributed to rapid variations in the modal parameters such as MS and CA. The absence of such rapid changes, however, does not exclude the possibility of notch formation. In this case, notch formation can still occur due to other factors. An example of this may be when two or more modes with similar MS values, but with different CA values, can cause a notch in a radiation pattern or impedance response. Consequently, it may be beneficial to consider the antenna surface current and characteristic mode analysis simultaneously.

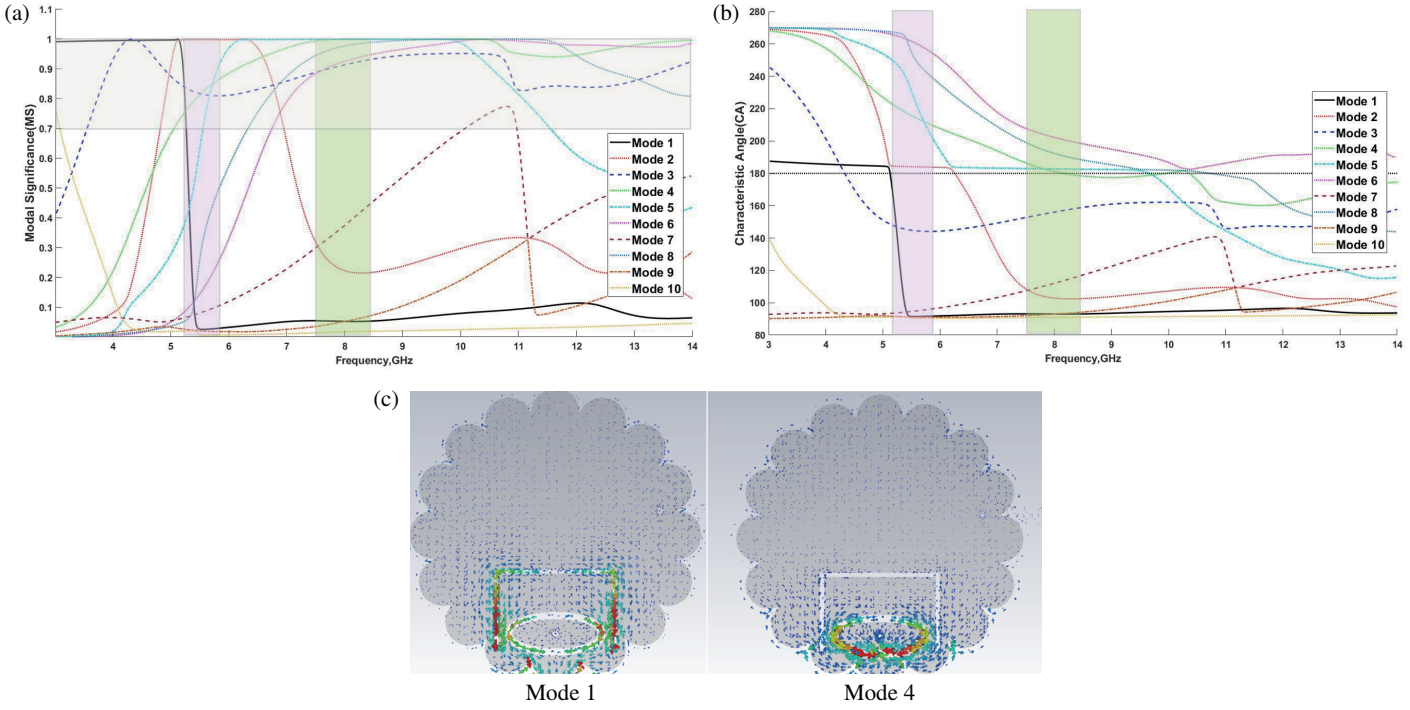


**FIGURE 6**. Characteristic mode analysis of the proposed antenna. (a) Modal Significance and (b) Characteristic angle (c) Antenna surface currents in modes 1 and 4.

## 4. RESULTS AND DISCUSSION

It is particularly challenging to design conventional antennas with a wide frequency range and a variety of new functions, such as tunable notches. Tuning of the second notch band is accomplished by changing bias voltages, which alters varactor diode capacitance ($C_{j0}$). Changing the bias voltage from 0 V to 12 V would result in moving the frequency of the second notch from 7.3 GHz to 8.7 GHz for simulation results. This frequency range is 7 GHz to 8.4 GHz for measurement results. Figs. 7(a) and (b) illustrate a final comparison between simulation and measurement results for $S$ parameters. The simulations typically assume perfect conditions, such as lossless materials, ideal connectors, and precise manufacturing tolerances, which are rarely achieved in reality. Due to measurement considerations such as bias circuit effects, including the SRF of the RF chokes, the impedance bandwidth in higher frequencies is limited. Additionally, there is also a little frequency shift caused by parasitic effects, model inaccuracies, and limitations in measurement setups. In the final measurement, the impedance bandwidth is 2.8 GHz to 13.2 GHz, with notch bands at 5.4 GHz and 7.9 GHz to 8.4 GHz. The realized gain of the antenna is simulated and measured at specific reverse bias voltages. In the UWB frequency range, gain is about 2 dBi but drops significantly at both the notch frequencies. Except for the notched frequency bands, the proposed design has an antenna efficiency ranging from 70% to 80%. The radiation pattern is another significant performance item. Inside an anechoic antenna chamber, radiation patterns are measured for two frequencies in both the $E$-plane and $H$-planem and the results of simulations and measurements of 2-D radiation patterns at 4 GHz and 9 GHz are presented in Figs. 7(c). A little variation about less than 1 dB in real pattern measurement is seen which can be eliminated using the smoothing mode in the network analyzer. Both frequencies exhibit bidirectional radiation patterns, whereas the $H$-plane radiation pattern exhibits omnidirectional behavior.

This paper presents a flower-shaped UWB monopole antenna. The frequency range can be tuned to other frequencies with changing the number of petals and consequently, the circumference of the antenna. Modifying the circumference of the patch reduces the lowest resonance frequency. The proper partial ground plane also improves the impedance bandwidth. For creating notch characteristic, U-shaped and elliptical slots are etched out from the radiating patch. The slot lengths and the capacitance range of the varactor diode are the tuning factors for changing the notched band frequency. The final dimension was optimized using CST Microwave Studio. Finally, a simple and compact antenna with a suitable gain and an omnidirectional pattern is proposed.

## 5. COMPARISON

Table 1 illustrates a comparison of the fabricated dual notched band UWB antenna with previous similar antennas. The proposed antenna has a simple structure, a wide tuning range for the second notch band, and an appropriate gain. The problem with the fixed band-notch solution is that it is permanent, and they cannot be dynamically adjusted. The first notch frequency is fixed in WLAN frequency band, and the second is tunable in X-band satellite communication. The proposed antenna has both tunable and fixed notched band configurations, each of which offers advantages in terms of dynamic adjustment and

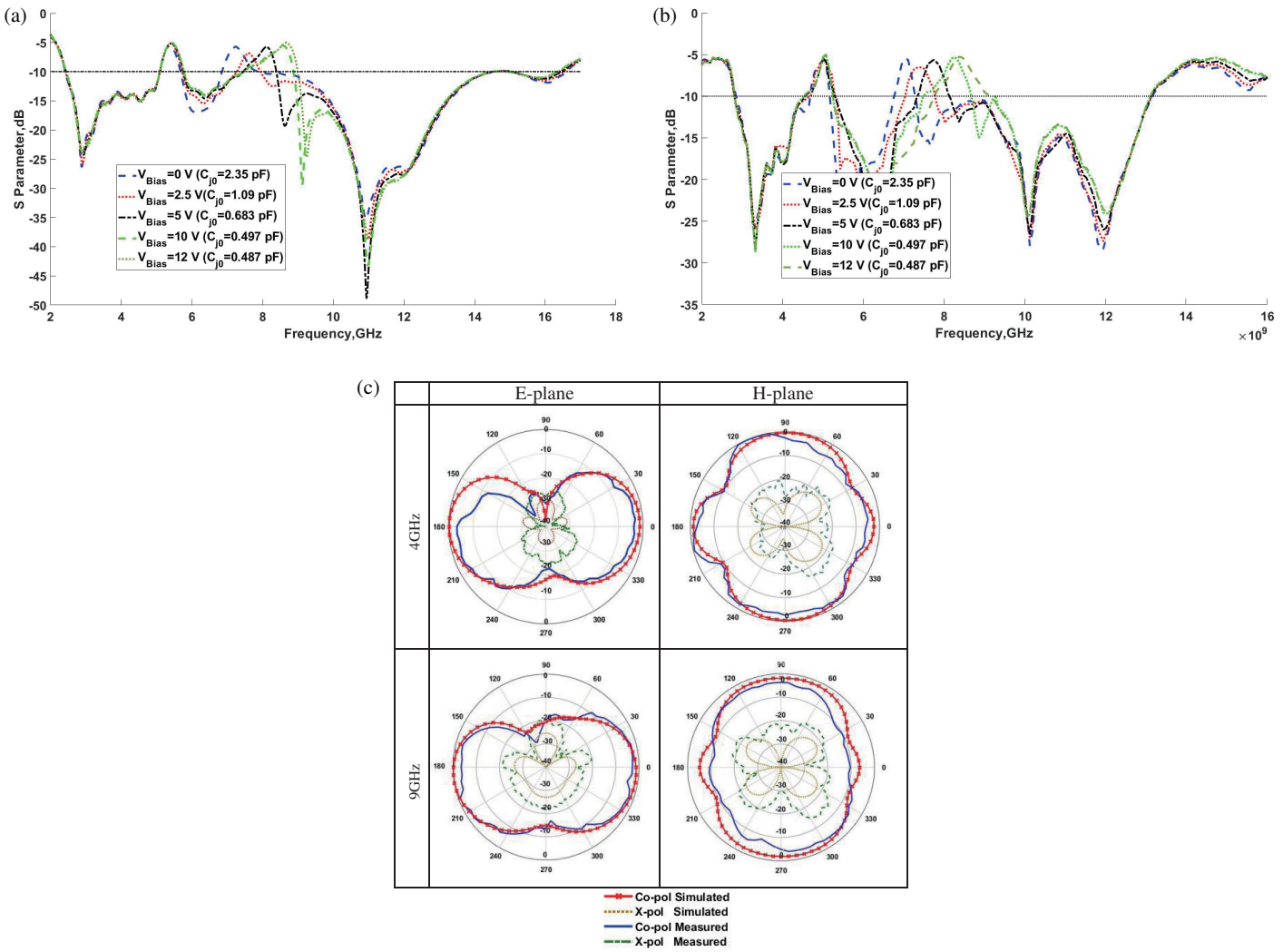


**FIGURE 7**. $S$-parameters of the designed dual notch band UWB antenna for several bias voltages $V_{Bias}$. (a) Simulated results. (b) Measured results. (c) Simulations and measurements of the 2-D radiation patterns for two frequencies, 4 GHz and 9 GHz.

**TABLE 1**. Comparison between some notched-band UWB antennas.

| Refs., Year | Size (mm$^3$) | BW (GHz) | Notch Characteristics | Tunability |
|---|---|---|---|---|
| [7], 2014 | $50 \times 50 \times 1.6$ | 3.1–10.6 | Single | No |
| [9], 2017 | $42 \times 50 \times 1.5$ | 3.1–10.6 | Dual | Yes |
| [16], 2021 | $30 \times 36 \times 0.7$ | 2.6–14 | Dual | Yes |
| [17], 2016 | $27 \times 34 \times 0.8$ | 3–11 | Dual | Yes |
| [26], 2018 | $34 \times 36 \times 1$ | 3.1–11 | Tri. | Yes |
| [31], 2020 | $27.1 \times 38.7 \times 1.6$ | 3.17–11.6 | Dual | Yes |
| [32], 2018 | $25 \times 30 \times 1.6$ | 2.4–12.8 | Dual | No |
| [33], 2021 | $30 \times 35 \times 0.8$ | 3.1–10.6 | Dual | No |
| [18], 2023 | $38 \times 59.5 \times 1.52$ | 3.1–11 | Dual | Yes |
| [34], 2023 | $30 \times 50 \times 1.6$ | 2.5–15 | Dual | No |
| [35], 2024 | $38 \times 30 \times 1.524$ | 2.9–14 | Single | No |
| This work | $25 \times 35 \times 1$ | 2.8–13.2 | Dual | Yes |

simplicity. Due to Table 1, the size of proposed antenna in comparison with previous papers with similar functionality is small. Although it is true that the existing references primarily focus on presenting a new antenna, this research has made a number of design innovations, including a compact size, the use of varactor diodes to tune notch bands, and the main objective of the paper is to verify the antenna using the CMA method.

## 6. CONCLUSION

This paper presents a dual-notched-band UWB antenna. In UWB antenna, some interfering bands cause communication distortion. To prevent the interference between WLAN (5.15–5.85 GHz) and X-band satellite communication links (7.9–8.4 GHz), dual-notch frequencies were achieved using two different slots on the radiating patch. The valuable characteristic of this paper is the use of a varactor diode in the elliptical slot to obtain tunable frequencies for the second notched band. For simulation and measurement, the impedance bandwidth is between 2.8 and 13.2 GHz except for notched-bands. On the basis of relevant equations, the antenna has been designed and simulated using CST Microwave Studio. A low-cost FR4 substrate is used for the antenna fabrication. FR4's lossy nature reduces suppression effect at notched frequencies. The results of the measurements, such as variations in reflection coefficients and far-field results, indicate good impedance matching, almost 2 dB gain, and a nearly omnidirectional pattern. A comparison of the gain difference between the passband and trap band shows a significant drop about 8 dB at the two notched frequencies. An ultra-wideband antenna design is proposed, which has been verified by CMA. This antenna is a dual-band-notched planar antenna with tunable characteristic. The antenna's performance was examined using the Characteristic Mode Analysis. The proposed antenna will be useful in a wide variety of modern UWB wireless systems.

## REFERENCES


[1] Federal Communications Commissions, "Federal Communications Commissions' rules regarding ultra-wideband transmission system from 3.1 to 10.6 GHz," Washington, DC, USA, 2002.

[2] Sarkar, D., K. V. Srivastava, and K. Saurav, "A compact microstrip-fed triple band-notched UWB monopole antenna," *IEEE Antennas and Wireless Propagation Letters*, Vol. 13, 396–399, 2014.

[3] Chandran, A. A. and S. Thankachan, "Triple frequency notch in UWB antenna with single ring SRR loading," *Procedia Computer Science*, Vol. 93, 94–100, 2016.

[4] Rizvi, S. N. R., W. A. Awan, D. Choi, N. Hussain, S. G. Park, and N. Kim, "A compact size antenna for extended UWB with WLAN notch band stub," *Applied Sciences*, Vol. 13, No. 7, 4271, 2023.

[5] Li, T., H. Zhai, G. Li, L. Li, and C. Liang, "Compact UWB band-notched antenna design using interdigital capacitance loading loop resonator," *IEEE Antennas and Wireless Propagation Letters*, Vol. 11, 724–727, 2012.

[6] Horestani, A. K., Z. Shaterian, J. Naqui, F. Martin, and C. Fumeaux, "Reconfigurable and tunable S-shaped split-ring resonators and application in band-notched UWB antennas," *IEEE Transactions on Antennas and Propagation*, Vol. 64, No. 9, 3766–3776, 2016.

[7] Siddiqui, J. Y., C. Saha, and Y. M. M. Antar, "Compact SRR loaded UWB circular monopole antenna with frequency notch characteristics," *IEEE Transactions on Antennas and Propagation*, Vol. 62, No. 8, 4015–4020, 2014.

[8] Jang, J.-W. and H.-Y. Hwang, "An improved band-rejection UWB antenna with resonant patches and a slot," *IEEE Antennas and Wireless Propagation Letters*, Vol. 8, 299–302, 2009.

[9] Xi, L., H. Zhai, Y. Zang, and L. Li, "A novel dual-band tunable band-notched antenna," *Microwave and Optical Technology Letters*, Vol. 59, No. 12, 3014–3018, 2017.

[10] Shome, P. P., T. Khan, and R. H. Laskar, "CSRR-loaded UWB monopole antenna with electronically tunable triple band-notch characteristics for cognitive radio applications," *Microwave and Optical Technology Letters*, Vol. 62, No. 9, 2919–2929, 2020.

[11] Jeong, M. J., N. Hussain, H.-U. Bong, J. W. Park, K. S. Shin, S. W. Lee, S. Y. Rhee, and N. Kim, "Ultrawideband microstrip patch antenna with quadruple band notch characteristic using negative permittivity unit cells," *Microwave and Optical Technology Letters*, Vol. 62, No. 2, 816–824, 2019.

[12] Ge, L., H. Liu, L. Tian, and Z. Li, "Design of novel patch quadruple band-notched UWB antenna," in *2022 IEEE 5th International Conference on Electronics Technology (ICET)*, 823–829, Chengdu, China, 2022.

[13] Ibrahim, A. A. and R. M. Shubair, "Reconfigurable band-notched UWB antenna for cognitive radio applications," in *2016 16th Mediterranean Microwave Symposium (MMS)*, 1–4, Abu Dhabi, United Arab Emirates, 2016.

[14] Salim, M. and A. Pourziad, "A novel reconfigurable spiral-shaped monopole antenna for biomedical applications," *Progress In Electromagnetics Research Letters*, Vol. 57, 79–84, 2015.

[15] Huff, G. H., J. Feng, S. Zhang, and J. T. Bernhard, "A novel radiation pattern and frequency reconfigurable single turn square spiral microstrip antenna," *IEEE Microwave and Wireless Components Letters*, Vol. 13, No. 2, 57–59, 2003.

[16] Rai, V. K. and M. Kumar, "Tunable inverted U-shaped dual band notch monopole antenna for ultrawideband applications," *IETE Journal of Research*, Vol. 69, No. 7, 4451–4460, 2021.

[17] Tang, M.-C., H. Wang, T. Deng, and R. W. Ziolkowski, "Compact planar ultrawideband antennas with continuously tunable, independent band-notched filters," *IEEE Transactions on Antennas and Propagation*, Vol. 64, No. 8, 3292–3301, 2016.

[18] Alazemi, A. J. and Y. T. Alsaleh, "An ultrawideband antenna with two independently tunable notch bands," *Alexandria Engineering Journal*, Vol. 79, 402–410, 2023.

[19] Chakraborty, M., S. Pal, and N. Chattoraj, "Quad notch UWB antenna using combination of slots and split-ring resonator," *International Journal of RF and Microwave Computer-Aided Engineering*, Vol. 30, No. 3, e22086, 2019.

[20] Moradi, N., F. Nazari, H. Aliakbarian, and F. A. Namin, "Compact ultrawideband monopole antenna with continuously tunable notch band characteristics," *Progress In Electromagnetics Research C*, Vol. 118, 71–81, 2022.

[21] CST Microwave Studio 2023, CST Gmbh (http://www.cst.com), 2023.

[22] Ray, K. P., "Design aspects of printed monopole antennas for ultra-wide band applications," *International Journal of Antennas and Propagation*, Vol. 2008, No. 1, 713858, 2008.

[23] Garg, R. K., M. V. D. Nair, S. Singhal, and R. Tomar, "A new type of compact ultra-wideband planar fractal antenna with WLAN band rejection," *Microwave and Optical Technology Letters*, Vol. 62, No. 7, 2537–2545, 2020.

[24] Mishra, B., R. K. Verma, N. Yashwanth, and R. K. Singh, "A review on microstrip patch antenna parameters of different geometry and bandwidth enhancement techniques," *International Journal of Microwave and Wireless Technologies*, Vol. 14, No. 5, 652–673, 2021.

[25] Deng, Z., C. Lai, Y. Wang, and K. Deng, "Design of a quadruple band-notched ultra-wideband (UWB) antenna using curled C-shaped structures and interdigital inductance slots," *Electronics*, Vol. 11, No. 23, 3949, 2022.

[26] Rahman, S. U., Q. Cao, Y. Li, I. Gil, and W. Yi, "Design of tri-notched UWB antenna based on elliptical and circular ring resonators," *International Journal of RF and Microwave Computer-Aided Engineering*, Vol. 29, No. 3, e21648, 2018.

[27] Skyworks Data Sheet, Skyworks Solutions, Inc., Available at www.skyworksinc.com.

[28] Murata Datasheet, Murata Manufacturing Co, Ltd. Available at www.murata.com.

[29] Garbacz, R. J., "Modal expansions for resonance scattering phenomena," *Proceedings of the IEEE*, Vol. 53, No. 8, 856–864, 1965.

[30] Addepalli, T., C. J. Rani, P. Nimmagadda, P. Badugu, J. b. Kamili, C. M. Kumar, P. Sunitha, and B. K. Kumar, "Design and analysis of UWB antenna with triple band notched characteristics verified with TCM analysis," *Wireless Personal Communications*, Vol. 134, No. 3, 1641–1664, 2024.

[31] Mayuri, P., N. D. Rani, N. B. Subrahmanyam, and B. T. P. Madhav, "Design and analysis of a compact reconfigurable dual band notched UWB antenna," *Progress In Electromagnetics Research C*, Vol. 98, 141–153, 2020.

[32] Singh, H. S. and S. Kalraiya, "Design and analysis of a compact WiMAX and WLAN band notched planar monopole antenna for UWB and bluetooth applications," *International Journal of RF and Microwave Computer-Aided Engineering*, Vol. 28, No. 9, e21432, 2018.

[33] Bao, S., W. Ren, Q. Zeng, Z. Xue, and W. Li, "An ultra-wideband multiple-input multiple-output antenna with dual band-notched characteristics," *International Journal of RF and Microwave Computer-Aided Engineering*, Vol. 32, No. 2, e22979, 2021.

[34] Rathore, P. S., R. Mali, R. Jatav, and M. K. Meshram, "A dual-band notched UWB antenna with a slot and a parasitic resonator," in *2023 IEEE Microwaves, Antennas, and Propagation Conference (MAPCON)*, 1–5, Ahmedabad, India, Dec. 2023.

[35] Mukherjee, S., A. Roy, A. Mukherjee, S. Kundu, P. P. Sarkar, and S. Bhunia, "Notch band characteristics improvement of a printed ultra wideband antenna by embedding frequency selective surface," *AEU — International Journal of Electronics and Communications*, Vol. 178, 155276, 2024.

[36] Zhou, Z. and K. L. Melde, "Frequency agility of broadband antennas integrated with a reconfigurable RF impedance tuner," *IEEE Antennas and Wireless Propagation Letters*, Vol. 6, 56–59, 2007.